

HIGH DENSITY Ti6Al4V VIA SLM PROCESSING: MICROSTRUCTURE AND MECHANICAL PROPERTIES

Chang-Jing Kong*, Christopher J. Tuck, Ian A. Ashcroft, Ricky D. Wildman and Richard Hague

Additive Manufacturing Research Group, Wolfson School of Mechanical and Manufacturing Engineering,
Loughborough University, LE11 3TU

REVIEWED, August 17 2011

Abstract

This paper investigates a density improvement method for Ti6Al4V alloy processed by the selective laser melting method. A modified inert gas inlet baffle has been employed to develop improved mechanical properties for these materials. Comparisons of the top surface and cross-section porosities of solid blocks processed by the original and modified gas inlet baffles indicate that the modified baffle greatly increases the properties of the processing blocks. Results showed that the porosity of the Ti6Al4V alloy was lower than 0.1% by area. The microstructure of the SLM Ti6Al4V alloy exhibited martensitic α' phase. The UTS tensile strength was 920-960MPa and the elongation at the fracture was 3-5%. The fracture surfaces of the tensile samples demonstrated a mixture of ductile and brittle fracture.

Introduction

Titanium alloys are extensively used in the aerospace and aeronautical [1], energy [2] and biomedical [3] industries due to its properties, such as high specific strength at elevated temperature, outstanding fracture resistance, excellent fatigue behavior, exceptional corrosion resistance and superior bio-compatibility. However, the complexity of the extraction process, difficulty of melting and problems during fabrication and machining of titanium alloys make them expensive compared to most other metals, which limits their application [4]. At present, most titanium parts are manufactured by conventional machining methods. All types of machining operations, such as turning, milling, drilling, reaming, tapping, sawing, and grinding, are utilized, which results in significant energy consumption and material wastage. In recent year, selective laser melting (SLM) processes have been developed to build components [5] with the advantage of being cost effective for producing one off parts with complex shape and structures [6]. Titanium alloys are some of the metal materials under investigation for SLM production [7-11]. As with many other SLM materials, the qualities of the components processed by the SLM methods produced a major concern as compared to those processed by hot work plus post heat treatment [7,12,13]. High-density SLM Ti6Al4V alloys cannot always be achieved due to the processing characteristics of the additive SLM process. Good bonding of the melted layers and lines is needed the issues to obtain high density within parts. Hence, it is necessary to understand the processing effects on the parts produced. Materials processed by the SLM process undergo a rapid cooling process. The microstructure of the Ti alloy processed by SLM will be different from those obtained with conventional manufacturing methods. This will also affect the mechanical properties of the components. It is therefore necessary to understand the microstructure and mechanical properties of titanium alloys processed by SLM. In this paper, the authors describe a method to improve the density of Ti6Al4V alloy components processed by SLM 250 system using a modified inert gas baffle. The high-density parts processed by the modified SLM have been metallographically and mechanically characterized.

Experimental Methods

The SLM equipment used was a SLM250 system from MTT Ltd, Which is shown schematically in Figure 1. A 200W laser was delivered through an optical train, which includes a variable focus lens,

* Corresponding author: email, C.Kong@lboro.ac.uk

galvanometer and F-theta lens before reaching the processing platform. The metal powders were spread on to the processing platform during the interval time of laser scanning. The processing chamber was sealed and evacuated before Argon gas was pumped in to provide an inert gas atmosphere. Throughout processing, the inert gas was circulated within the processing chamber by using an extractor pump to take gas out of the processing chamber on the left side, and deliver it back through the right side baffle. Oxygen sensors were used to ensure that the O₂ was below 900ppm at all times. If the oxygen level was higher than this value, the inert gas valve opens to refill more argon gas into the chamber.

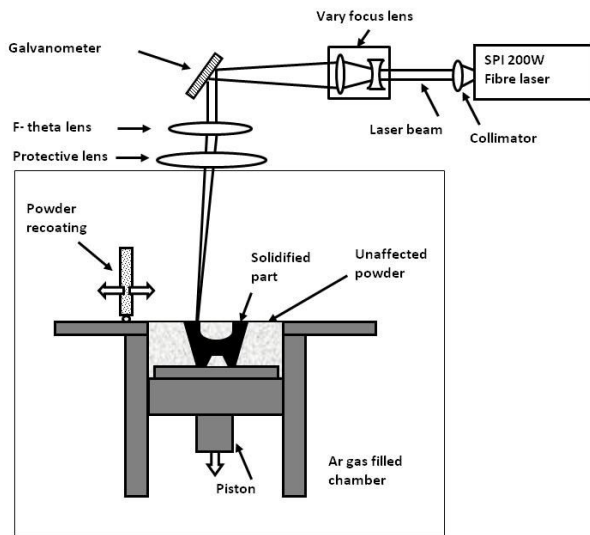


Figure 1. Schematic image of the SLM250 system

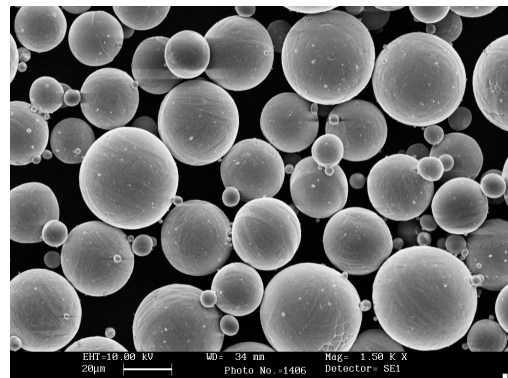


Figure 2. Plasma gas atomized Ti6Al4V powder

Plasma atomized Ti6Al4V powder (provided by LPW Ltd., UK) was used to process thin wall and solid blocks using the SLM250 system. Figure 2 shows an SEM image of the powder. Experiments were carried out on both the original inert gas inlet baffle and a modified thin slit gas inlet baffle (Figure 3). The gap of the thin slit was 300µm (Figure 3b).

Thin walls were processed at a ‘real’ laser power of 177W, laser exposure point distance of 50-70µm and laser pulse exposure time of 60-371µs. The thin wall thickness was measured using vernier callipers. Solid blocks with dimensions of 10 × 12 × 10 mm³ were processed at a laser power of 177W, point distance of 60-65µm, laser pulse exposure time of 60-371µs and hatch spacing of 100-280 µm. The layer thickness was 50µm and the platform background temperature was 150°C. The scanning strategy used was ‘meander scanning’, in which the scanning direction rotates 67° clockwise for each layer.

Optical microscopy, field emission gun scanning electron microscopy (SEM) and energy dispersive X-ray spectroscopy (EDX) were used to analyze the powder, thin walls, and the top surface and cross sections of the individual solid blocks. X-ray was used to check the metallographic phase of Ti6Al4V alloy’s powder and solid blocks. The samples were cross-sectioned perpendicular to the blocks and the porosity percentages of the blocks were recorded using a low magnification optical microscopy. Recorded images were processed by software to obtain a statistical measurement on porosity percentage of the viewed areas. Cross-sectioned samples were etched using Kroll’s reagent with a composition of 3ml HF, 6ml HNO₃ and 100ml distilled water according to standard ASTM E407-07 and observed by optical microscope. The microhardness was tested with a load of 500 gram and duration time of 15 second.

Tensile tests were performed using an Instron 3369 tensile system (Instron Ltd, Bucks, UK). The tensile samples were designed according to standard ASTM E8/E8M-09 with the subsize specimen, i.e. width of 6mm. The thickness of the samples was 3mm. Tensile specimens were processed on the platform in the direction of X,

Y and Z direction. Five samples were prepared in each processing direction. The ultimate tensile strength, yield strength and the elongation values are the average values of the test.

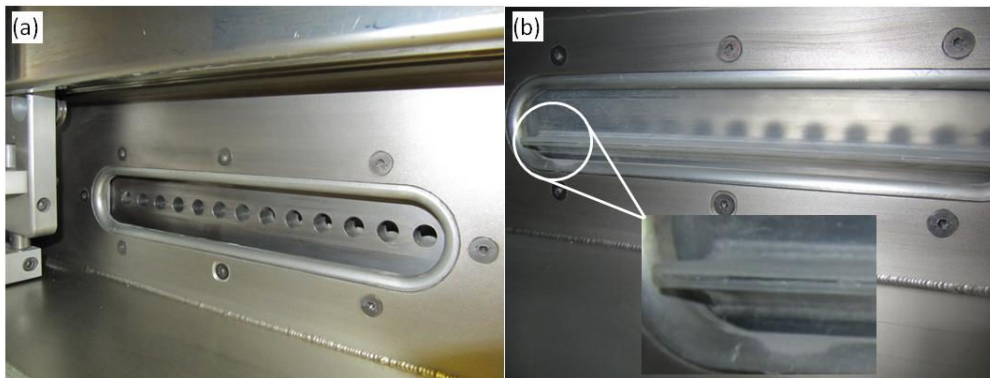


Figure 3. Inert gas inlet baffle on the processing chamber. (a) Original baffle, pump at 24Hz; (b) Thin slit baffle, pump at 13Hz.

Results and Discussion

The initial experiments were carried out using the original inert gas inlet baffle (Figure 3a). In order to optimize the processing parameters, thin walls were processed to find the possible parameters to build solid blocks. Figure 4 shows the relationship between thin wall thickness and energy input. The results indicate an approximately proportional relationship between energy input and thin wall thickness. The energy input per unit length is the control factor for the wall thickness. The completed full height thin walls were on those energy inputs higher than 0.45Jmm^{-1} .

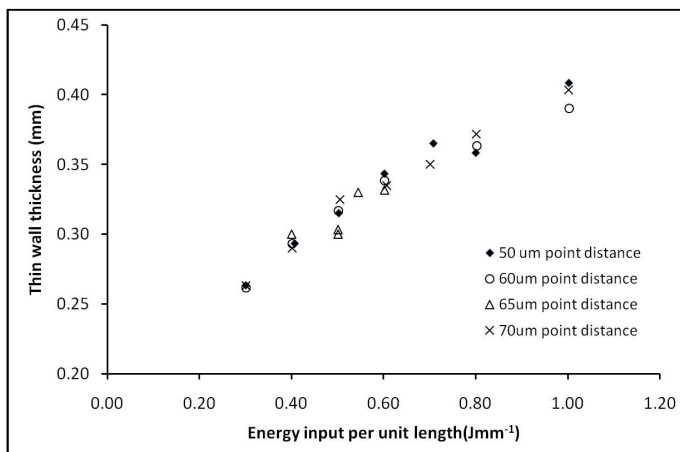


Figure 4. Relationship between energy input per unit length and the thin wall thickness

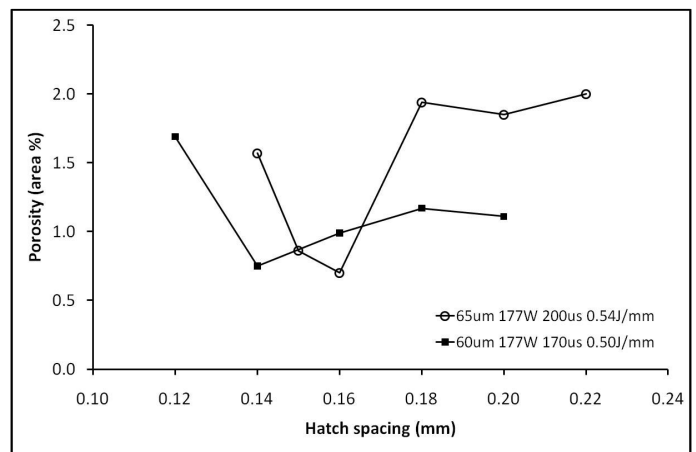


Figure 5. Hatch spacing and the porosity percentage

Solid blocks were processed at laser power of 177W, point distances of 65 and 60 μm , exposure times of 200 μm and 170 μm on various hatch spacings. The energy input per unit length was 0.54 and 0.50 Jmm^{-1} respectively. The porosity percentage vs. hatch spacing is shown in Figure 5. Minimum porosity percentages were acquired with hatch spacings of 140 or 160 μm , depending on the energy input. Samples processed at a laser power of 177W, point distance of 65 μm , laser exposure time of 200 μs and hatch spacing 160 μm , which has a minimum porosity percentage, was examined both on the top surface (Figure 6a) and the cross-section (Figure 6b) of the block. The largest pores reached 500 μm . In order to reduce the porosity percentage, more experiments were

carried out at the increased the energy input with various hatch spacings. However, surface morphology observation of the samples (images are not show in this paper) gave no trend of pores to the hatch spacing variation. It was found that the samples on the left side (close to the inert gas extraction side) had better surface quality than those on the right side (close to the inert gas inlet position).

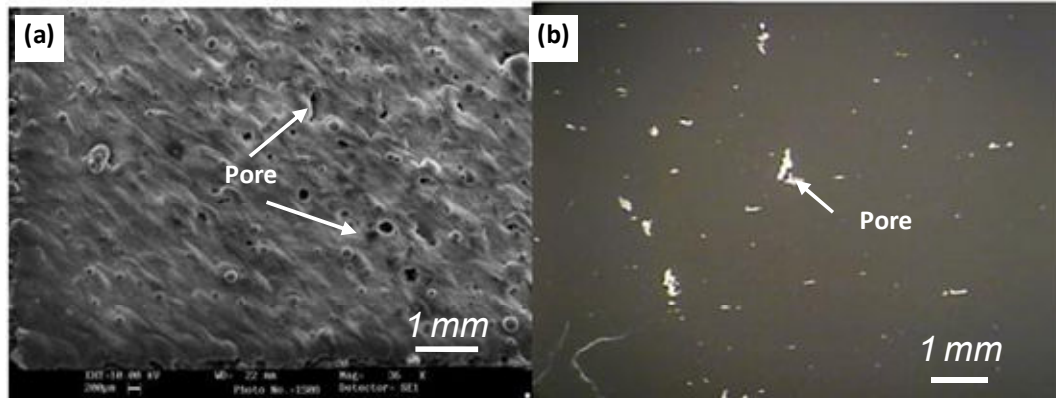


Figure 6. Large pores on top surface and in the cross section of the blocks

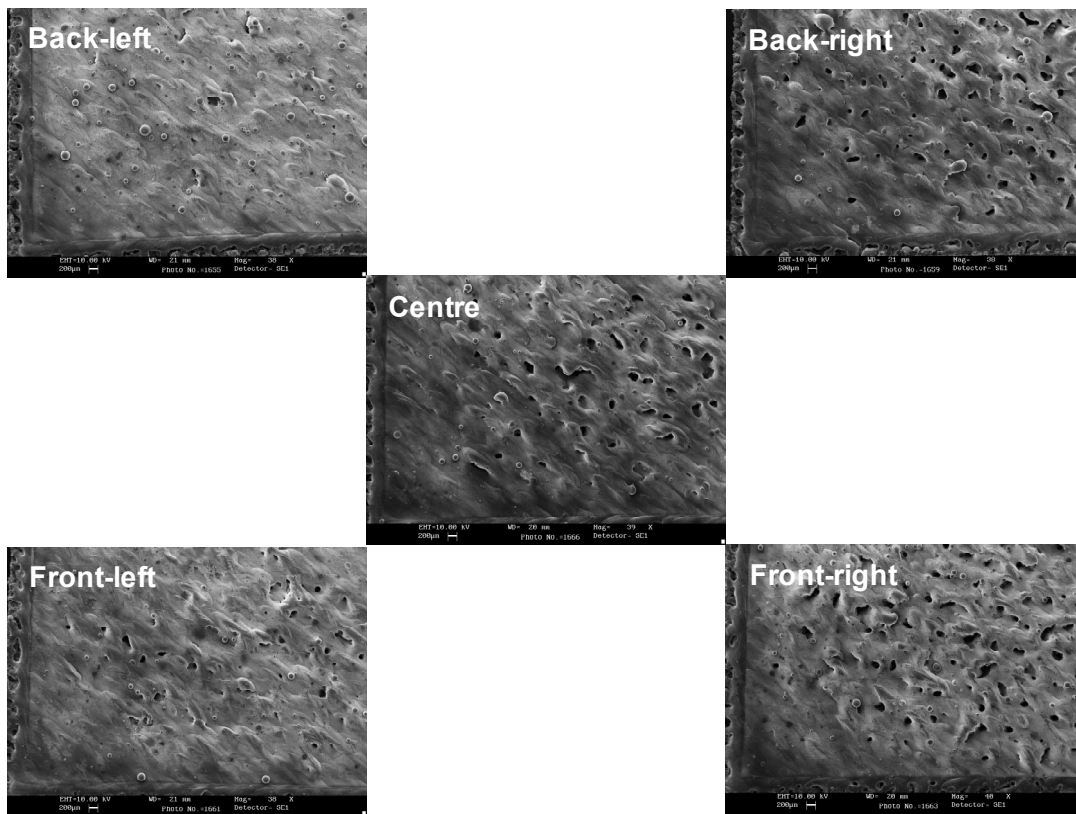


Figure 7. SEM top surface morphology of the position effect with original gas inlet baffle

To verify the position effect on the processing platform, an experiment was designed to put samples on the four corners and the center of the platform. The same processing parameters were used at a laser power of 177W, point distance of $60\mu\text{m}$, exposure time of $185\mu\text{s}$ and hatch spacing of $140\mu\text{m}$. The surface SEM morphology (Figure 7) indicates that position affects the surface qualities of these blocks. Samples close to the inert gas extraction (left side of platform) had better surface quality than samples on the centre and samples close to the inert gas inlet side (right side of platform).

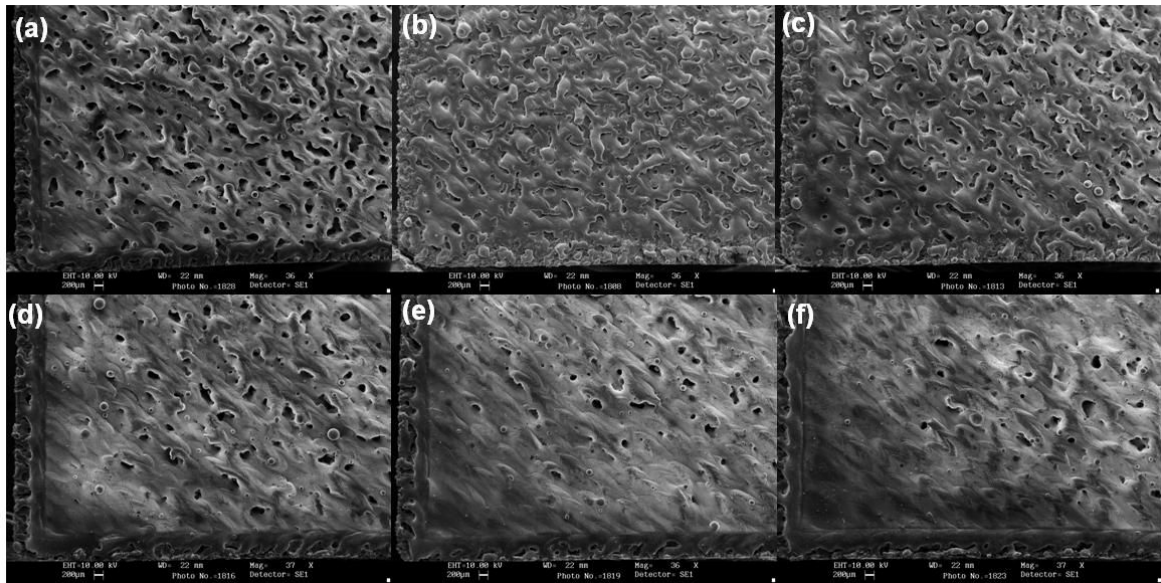


Figure 8. Top surface morphology of the samples processed using MTT's original gas inlet baffle (a) 0.45J/mm, (b) 0.55J/mm, (c) 0.60J/mm, (d) 0.70J/mm, (e) 0.80/mm, (f) 1.0J/mm

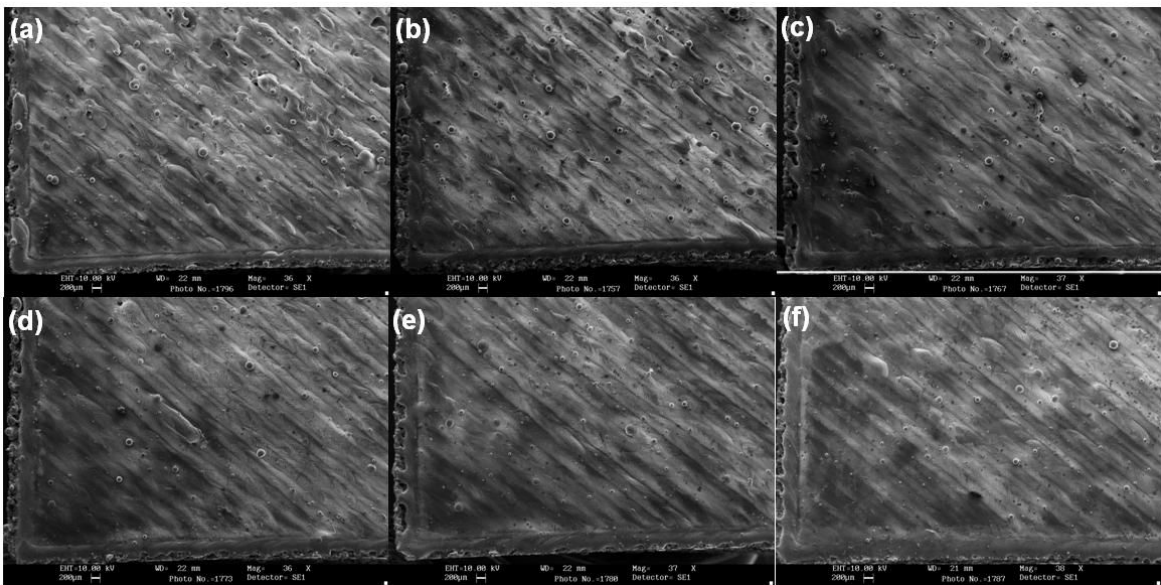


Figure 9. Top surface morphology of the samples processed using the modified thin slit gas inlet baffle (a) 0.45J/mm, (b) 0.55J/mm, (c) 0.60J/mm, (d) 0.70J/mm, (e) 0.80/mm, (f) 1.0J/mm

In order to test the effect of the gas inlet baffles (shown in Figure 3), experiments were processed with the original inert gas inlet baffle and the modified thin slit inert gas inlet baffle. The same series of processing parameters and sample position were used with a laser power of 177W, point distance of $50\mu\text{m}$, exposure times of $127\text{-}155\mu\text{s}$ and hatch spacing of $180\mu\text{m}$. Samples were put on the centre of the processing platform for both experiments. The surface morphology of the samples processed using the MTT's original gas inlet baffle and the modified thin slit gas inlet baffle are shown in Figures 8 and 9. The results indicate that using the original MTT gas inlet baffle, increasing the energy input can reduce the number of the top pores on the samples (Figure 8), but the pore size is still large even with a high energy input (Figure 8f). Conversely, smooth surfaces can be obtained at almost every set energy input when using the modified thin slit inert gas inlet baffle (Figure 9). A possible reason for the thin slit gas inlet baffle having an effect on increasing the surface quality may be because it provides greater gas velocity across the build envelope. The gas flow with this design can more

effectively remove fume and fine powders during processing. These fume and fine powders floating within the chamber can block the laser energy during processing and when they deposit on the protective lens a further reduction on the input laser energy occurs.

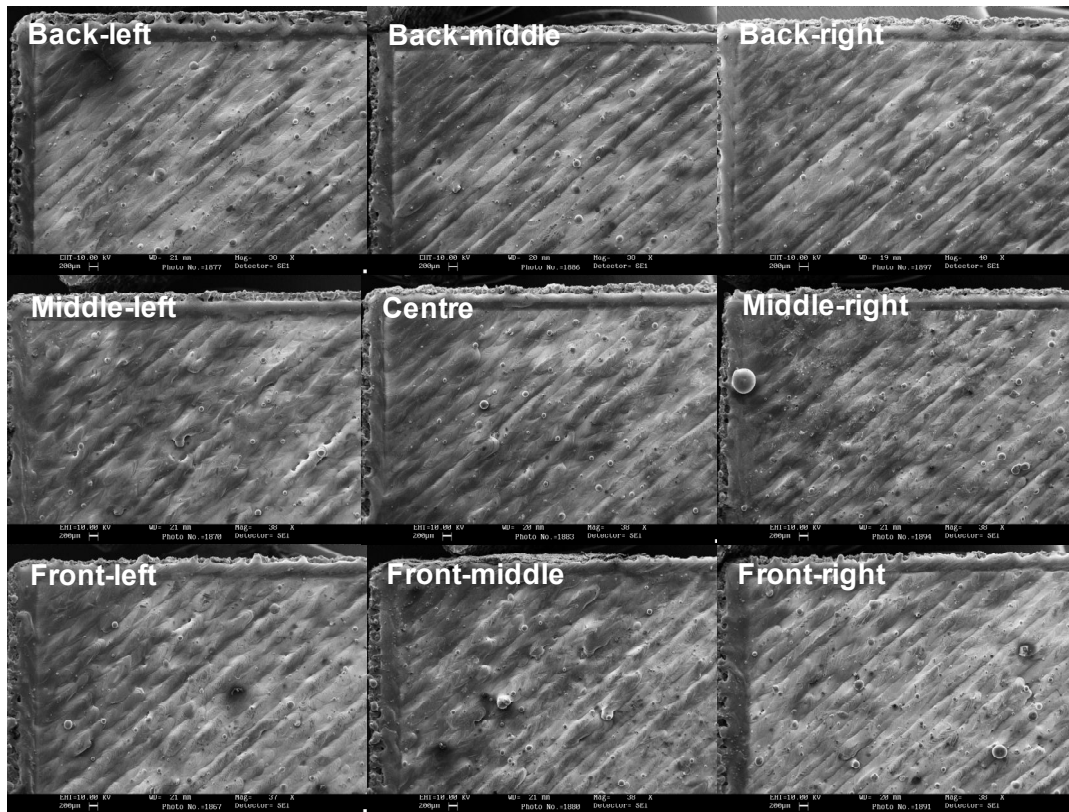


Figure 10. SEM top surface morphology of the position effect with the modified thin slit gas inlet baffle

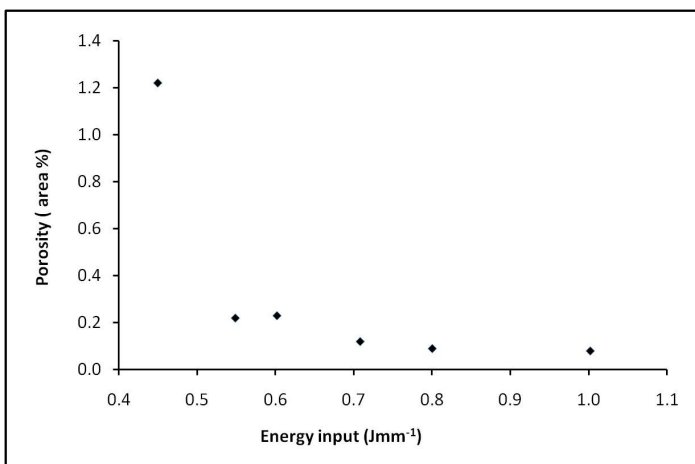


Figure 11. Energy input per unit length vs. porosity % with thin slit baffle

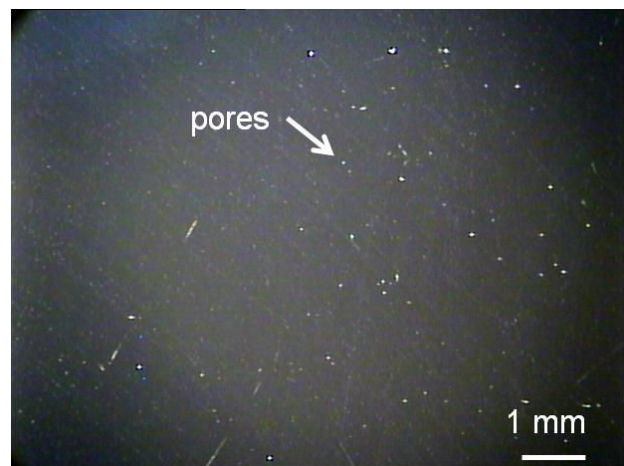


Figure 12. Cross-section image of block processed with thin slit baffle

To test the position effect samples built with modified thin slit gas inlet baffle, an experiment was designed with samples on the centre, four corners and four sides of the platform with the same processing parameters of laser power of 177W, point distance of 50µm, exposure time of 226µm, hatch spacing of 180µm. The surface morphologies of the samples are shown in Figure 10. No position effect can be observed on the samples processed using the thin slit gas inlet baffle.

The porosity percentage of samples processed using the thin slit gas inlet baffle vs. energy input is shown in Figure 11. The porosity percentage decreases with energy input increases. The lowest porosity achieved was 0.1% in area. Cross-section images show that the porosity sizes are much smaller than seen in those samples processed using the original gas inlet baffle. Figure 12 is an example of a sample processed using the thin slit gas inlet baffle. The processing parameters was of laser power of 177W, point distance of 50 μm , laser exposure time of 200 μs and the hatch spacing of 180 μm . The pore (white) sizes in the sample processed using the thin slit gas inlet baffle (Figure 12) are much smaller (less than 100 μm) than those seen in sample processed using the original gas inlet baffle (Figure 6b).

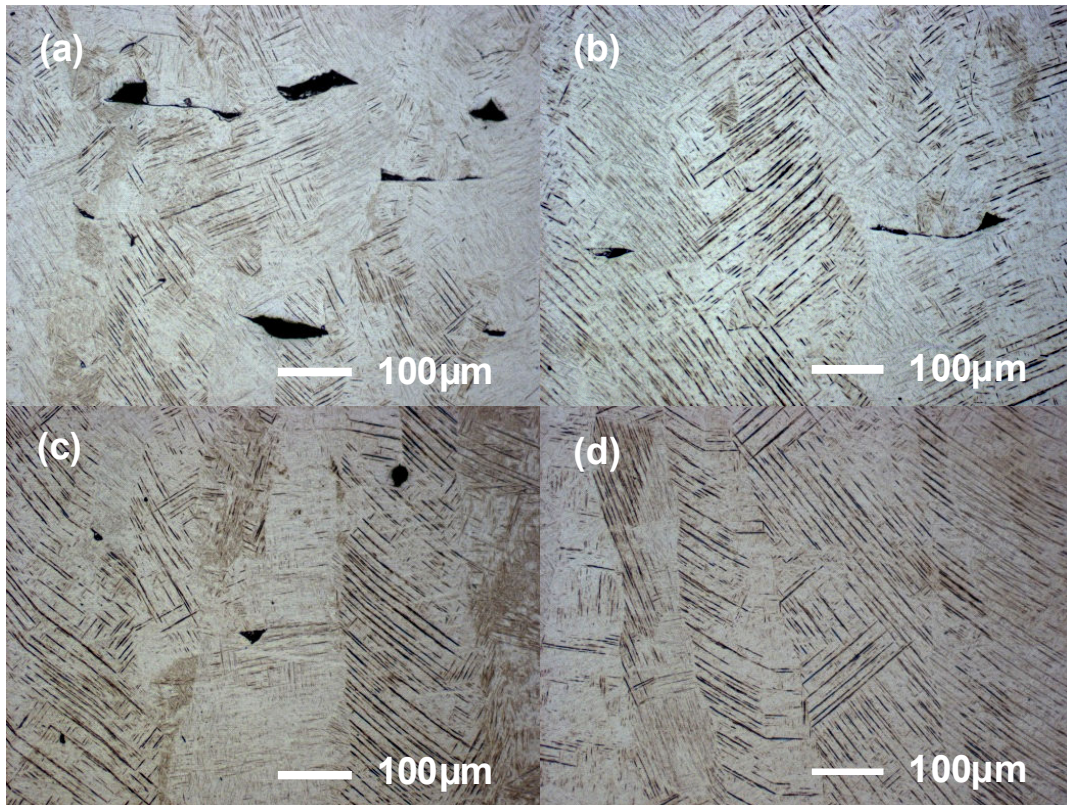


Figure 13. Microstructure of Ti6AlV SLM solid blocks. (a) 0.45J/mm (b) 0.60J/mm (c) 0.8J/mm (d) 1.0 J/mm

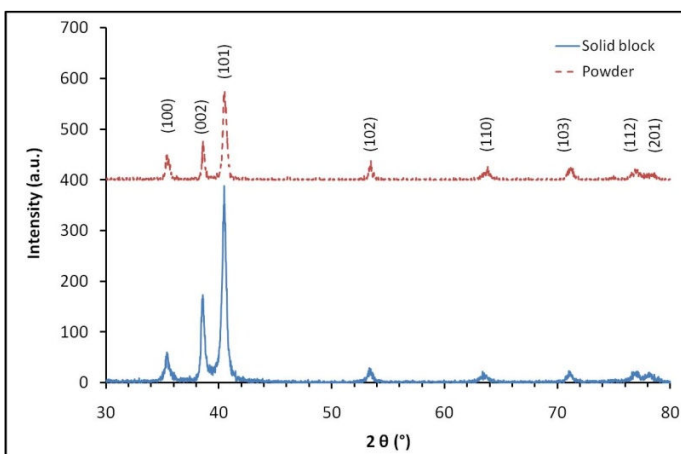


Figure 14. XRD pattern of the powder and solid block
Solid block processed at 0.8Jmm⁻¹

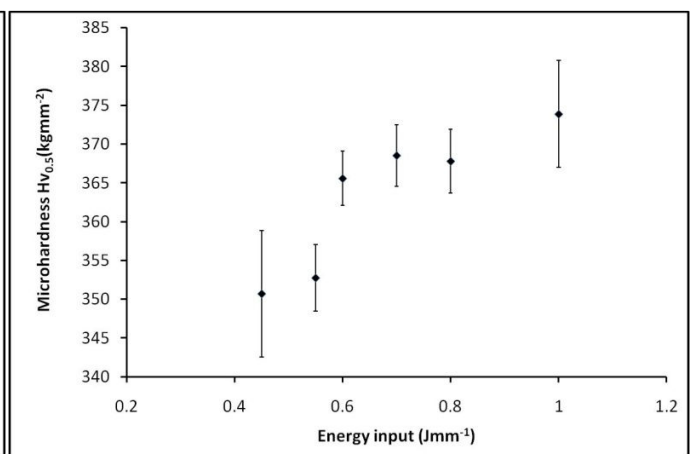


Figure 15. the energy input vs. microhardness

Microstructures of the samples processed using the thin slit gas inlet baffle are shown in Figure 13. Elongated grains are observed growing through the deposition layers (50 μ m). Martensite plates are visible within the grains, which is consistent with results by other authors [7,9]. The pores formed when using a low energy input (Figure 13 a-c) are mainly due to the lack of bonding between layers. X-ray diffraction spectra (Figure 14) indicate the presence of hcp (α' martensite) phase only, on both the powder and selective laser melted solid block processed with an energy input of 0.8Jmm⁻¹[7,9,14]. The microhardness results from these samples are shown in Figure 15. The microhardness values increase with energy input. The possible reason for this is the reduction of the porosity within the samples (Figure 11 & 13).

The tensile testing results are shown in Table 1 and the initial areas of the strain-stress curve for samples prepared in Y and Z directions are shown in Figure 16. The yield strength (on 0.2% offset) and ultimate tensile strength of the testing results are lower than those by other authors and the elongation at fracture values are similar [8,9]. The fracture morphology in the samples prepared in the X, Y and Z direction are very similar. Figure 17 shows the fracture structure of a sample prepared in the Y-direction. Mixture of ductile fracture (dimple network) and brittle fracture (cleave and shear lip region) was found. The un-melted pores within the tensile testing samples may be one of the reasons for the reduction of the YS and UTS compared with others results [8, 9].

Table 1. Tensile test results of the Ti6Al4V alloy in different processing directions

SLM250	Average YS 0.2% offset Mpa	Average UTS Mpa	Average Elongation %
X-direction		938 \pm 8.1	3.90 \pm 0.73
Y-direction	800	967 \pm 11	3.45 \pm 0.19
Z-direction	770	920 \pm 5.2	4.44 \pm 0.94

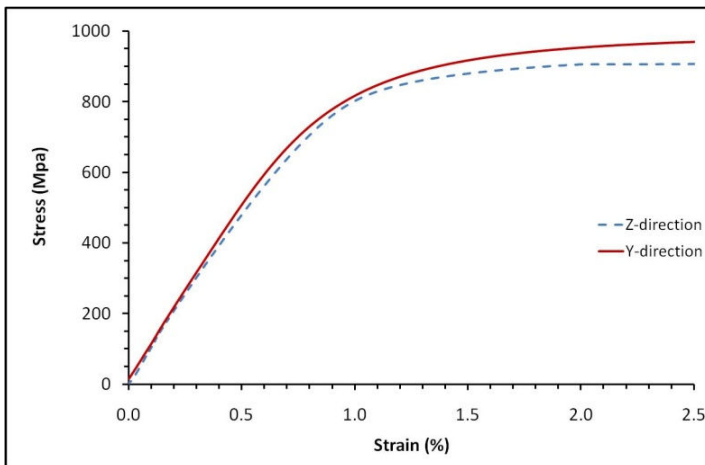


Figure 16. Strain-stress curves of for samples prepared in Y and Z direction

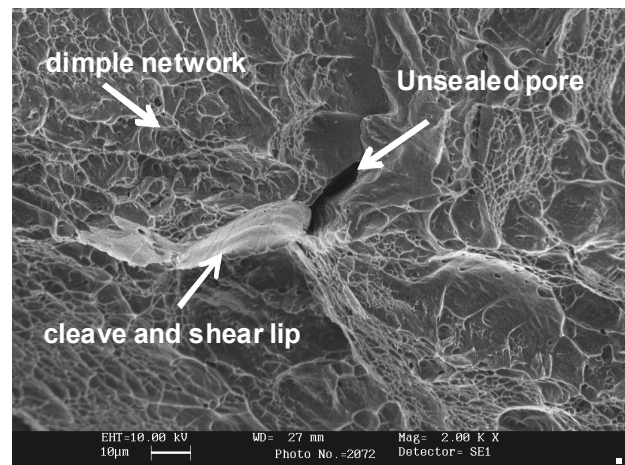


Figure 17. Fracture structure of samples built in the Y direction sample

Conclusions

A modified thin slit gas inlet baffle was seen to solve the problem of the position effect for the samples in different areas of the platform. It also reduced the percentage and size of pores in solid blocks. The lowest porosity percentage of 0.10% was seen in sample with an energy input of 1.0 Jmm⁻¹ and its microhardness was 375 gmm⁻². The microstructure of the solid blocks were hcp α' martensite phase. The UTS was 920-960MPa

and elongation was 3-5%. The fracture structure was a mixture of dimple networks, cleave and shear lip regions.

References

1. R.R. Boyer, An overview on the use of titanium in the aerospace industry, *Materials Science and Engineering*, A213 (1996) pp103-114
2. R.W. Schutz, H.B. Watkins, Recent developments in titanium alloy application in the energy industry, *Materials Science and Engineering* A243 (1998) pp305–315
3. H.J. Rack, J.I. Qazi, Titanium alloys for biomedical applications, *Materials Science and Engineering C* 26 (2006) 1269 – 1277
4. E.O. Ezugwu, Z.M. Wang, Titanium alloys and their machinability a review, *Journal of Materials Processing Technology* 68 (1997) 262-274
5. http://ec.europa.eu/clima/policies/g-gas/index_en.htm
6. R. HAGUE, S. MANSOUR and N. SALEH, Material and design considerations for Rapid Manufacturing, *International Journal of Production Research*, Vol. 42, No. 22, (2004) pp4691–4708
7. Lore Thijs, Frederik Verhaeghe, Tom Craeghs, Jan Van Humbeeck, Jean-Pierre Kruth, A study of the microstructural evolution during selective laser melting of Ti–6Al–4V, *Acta Materialia* 58 (2010) 3303–3312
8. L.E. Murra, S.A. Quinonesb, S.M. Gaytana, M.I. Lopeza, A. Rodelaa, E.Y. Martineza, D.H. Hernandez, E. Martineza, F. Medinac, R.B. Wickerc, Microstructure and mechanical behavior of Ti–6Al–4V produced by rapid-layer manufacturing, for biomedical applications, *Journal of The Mechanical Behaviour of Biomedical Materials*, 2 (2009) 20-32 EBM
9. Luca Facchini, Emanuele Magalini, Pierfrancesco Robotti, Alberto Molinari, Simon Hoßges, Konrad Wissenbach, Ductility of a Ti-6Al-4V alloy produced by selective laser melting of prealloyed powders, *Rapid Prototyping Journal* 16/6 (2010) 450–459
10. P.A. Kobryn and S.L. Semiatin, The Laser Additive Manufacture of Ti-6Al-4V, *JOM*, 2001 September, 40-42
11. Patrick H. Warnke, Timothy Douglas, Patrick Wollny, Eugene Sherry, Martin Steiner, Sebastian Galonska, Stephan T. Becker, Ingo N. Springer, Jorg Wiltfang, and Sureshan Sivananthan, Rapid Prototyping: Porous Titanium Alloy Scaffolds Produced by Selective Laser Melting for Bone Tissue Engineering, *Tissue Engineering: Part C* 15(2), (2009) pp115-124
12. Ben Vandenbroucke and Jean-Pierre Kruth, Selective laser melting of biocompatible metals for rapid manufacturing of medical parts, *Rapid Prototyping Journal*, 13/4 (2007) 196–203
13. F Abe, E Costa Santos, Y Kitamura, K Osakada and M Shiomi, Influence of forming conditions on the titanium model in rapid prototyping with the selective laser melting process, *Journal of Mechanical Engineering Science*, Proceeding of Institute of Mechanical Engineering Vol. 217 Part C: C01502 (2003) pp119-126
14. M.T. Jovanovic, S. Tadic, S. Zec, Z. Miskovic and I. Bobic, The effect of annealing temperatures and cooling rates on microstructure and mechanical properties of investment cast Ti–6Al–4V alloy, *Materials and Design* 27 (2006) pp192–19